ADVANCING EARTH AND SPACE SCIENCES

Geophysical Research Letters

RESEARCH LETTER

10.1029/2024GL109645

Key Points:

- Sheared granular halite exhibits constant friction at small slip displacement and substantial weakening at large displacement
- Characteristic slip lengths for constant friction and weakening decrease with normal stress and are characterized by similar exponents
- The production, saturation, and overflow of comminuted fines in the shear zone are key factors determining transient frictional behavior

Supporting Information:

Supporting Information may be found in the online version of this article.

Correspondence to:

T. Yamaguchi,
yamaguchi-tetsuo@g.ecc.u-tokyo.ac.jp

Citation:

Chang, C., Noda, H., Hamada, Y., Huang, C., Ma, T., Wang, G., & Yamaguchi, T. (2024). Comminution-induced transient frictional behavior in sheared granular halite. *Geophysical Research Letters*, *51*, e2024GL109645. https://doi.org/10.1029/2024GL109645

Received 5 APR 2024
Accepted 25 SEP 2024

Author Contributions:

Conceptualization: Chengrui Chang, Hiroyuki Noda, Yohei Hamada, Chao Huang, Tao Ma, Tetsuo Yamaguchi
Formal analysis: Chengrui Chang, Tao Ma
Funding acquisition: Tetsuo Yamaguchi
Investigation: Chengrui Chang, Chao Huang
Methodology: Chengrui Chang, Hiroyuki Noda, Yohei Hamada, Tetsuo Yamaguchi
Resources: Gonghui Wang
Software: Tao Ma
Writing – original draft: Chengrui Chang, Tetsuo Yamaguchi

Comminution-Induced Transient Frictional Behavior in Sheared Granular Halite

Chengrui Chang[1], Hiroyuki Noda[2], Yohei Hamada[3], Chao Huang[4], Tao Ma[5], Gonghui Wang[2], and Tetsuo Yamaguchi[1]

[1]Department of Biomaterial Sciences, Graduate School of Agricultural and Life Sciences, The University of Tokyo, Tokyo, Japan, [2]Disaster Prevention Research Institute, Kyoto University, Uji, Japan, [3]Kochi Institute for Core Sample Research, Japan Agency for Marine-Earth Science and Technology (JAMSTEC), Nankoku, Japan, [4]Division of Earth and Planetary Sciences, Graduate School of Science, Kyoto University, Uji, Japan, [5]Institute of Modern Physics, Chinese Academy of Sciences, Lanzhou, China

Abstract Grain comminution is commonly observed in numerous geological settings. To elucidate the role of grain comminution in dry granular friction, we sheared breakable halite (NaCl) grains using a ring-shear configuration at a constant slip rate under various normal stresses. We observed transient frictional behaviors: a constant regime exhibiting a high friction coefficient at small slip displacements, and a weakening regime showing a substantial decay in friction at large slip displacements. The characteristic slip lengths for both regimes decreased with normal stress and were characterized by similar exponents. Micro-X-ray tomography revealed the evolution of microstructure from distributed grain comminution to progressive shear localization for these two regimes. We propose that the filling processes of comminuted fine particles, during which fine particles saturate and then overflow the shear zone, define transient frictional behaviors. This study may hold significant implications for natural shear systems, given the ubiquity of comminution and localization phenomena.

Plain Language Summary Grain comminution and structural evolution are common phenomena in natural settings, including earthquake faults and landslides. However, their role in granular friction remains unclear. To investigate this, we experimentally sheared breakable NaCl grains to simulate the processes within growing fault zones and visualized microstructural evolution using micro-X-ray computed tomography (CT). We observed two distinct frictional behaviors: a constant regime exhibiting a high friction coefficient at small slip displacements, and a weakening regime showing a substantial decay in friction at large slip displacements. The characteristic slip lengths for both regimes decreased with normal stress. Micro-observations revealed drastic grain comminution and segregation processes in the constant regime, while the weakening regime showed progressive shear localization evolving from multiple discontinuous shear planes to one extremely localized shear plane. The higher constant friction appeared to result from large grain contacts, while the substantially lower steady-state friction arose from comminuted fine particle contacts. We propose that grain comminution generates fine particles, gradually filling the pores within the shear zone in the constant regime, ultimately leading to frictional weakening by effectively reducing large grain contacts. The characteristic lengths defining transient behavior may be influenced by geometrical complexities and boundary conditions in various geological settings.

1. Introduction

The constitutive properties and frictional behavior of faults are key factors in understanding diverse faulting processes. Many experimental studies have been conducted using various configurations such as double direct shear (e.g., Dieterich, 1972, 1978), rotary shear (e.g., Tsutsumi & Shimamoto, 1997; Weeks & Tullis, 1985), triaxial shear (cylinder with ~35° sawcut; e.g., Brace & Byerlee, 1966; Shimamoto et al., 1980), and large-scale biaxial friction (e.g., Dieterich, 1981; Mclaskey & Yamashita, 2017; Yamashita et al., 2015). In these experimental studies, the shear zone thickness was in the order of several millimeters and could not increase owing to restricted slip displacement or gouge confinement. In contrast, the gouge thickness in natural faults is usually much greater than that in experimental faults (e.g., Chambon et al., 2006; Engelder, 1974; Robertson, 1982; Scholz, 1987) and the energy dissipation and rupture processes within a thick layer differ from those at a distinct interface (Sibson, 2003). Furthermore, while most experimental configurations include gouges sandwiched

Writing – review & editing: Chengrui Chang, Hiroyuki Noda, Yohei Hamada, Chao Huang, Tetsuo Yamaguchi

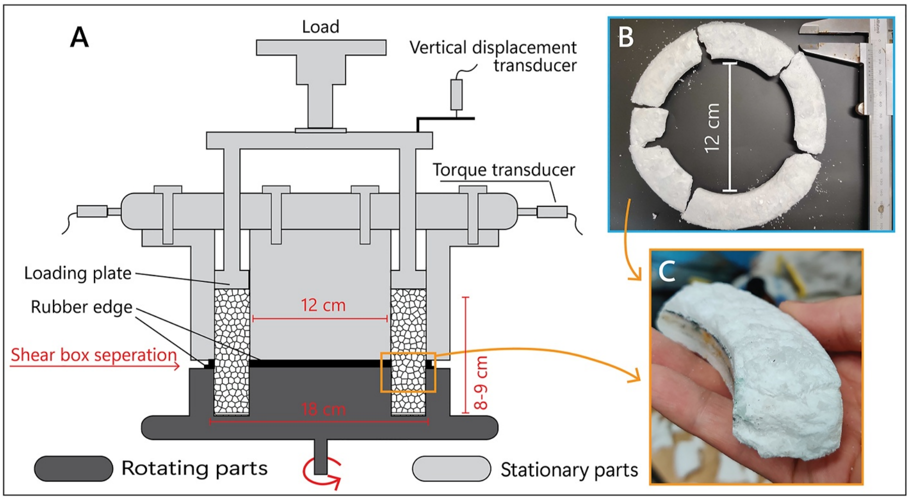

Figure 1. Ring-shear configuration and shear zones after test. (a) Depiction of ring-shear apparatus. (b) Top view of shear zone samples for coarse-grained medium. (c) Shear zone block of coarse-grained medium.

between consolidated host rocks, few studies have investigated the effects of unconsolidated and highly porous rocks and sediments, which are frequently involved in upper crust faults (e.g., Chester & Logan, 1986; Faulkner et al., 2010) and subduction zones (e.g., Kitajima & Saffer, 2014; Polet & Kanamori, 2000).

The cataclastic process is active in faulting processes and stimulates intense fracturing and crushing of grains (e.g., Borg et al., 1960; Engelder, 1974; Fossen, 2010; Griggs & Handin, 1960; Kimura et al., 2007). Apart from earthquake faults, large rock avalanches are another significant geophysical phenomenon that often exhibit thick deposits accompanied by extreme grain size reduction (e.g., Crosta et al., 2007; Davies et al., 1999; T. R. Davies and McSaveney, 2002, 2009; Heim, 1932) and result in large runouts (e.g., T. R. H. Davies, 1982; Davies et al., 1999; Heim, 1932; Hsü, 1975; Legros, 2002). Although their geometries, boundary conditions, and stress levels differ significantly from those of earthquake faults, shearing of dense granular flow is common (e.g., Siman-Tov & Brodsky, 2018), and the fine particles produced are considered to play an important role in the friction of the fault zone.

In this study, we aim to elucidate the mechanisms of grain comminution and structural evolution in a growing fault zone developing in an unconsolidated and porous granular medium. Friction experiments were performed using a ring shear apparatus (Sassa et al., 2004) and a large volume of breakable grains. Halite (NaCl) has been frequently used as an analogue material for cataclastic and brittle-ductile deformation because it reveals a wide variety of deformation mechanisms (e.g., Bos & Spiers, 2002; Buijze et al., 2017; Chester & Logan, 1990; Hiraga & Shimamoto, 1987; Kim et al., 2010; Noda & Shimamoto, 2010, 2012; Shimamoto, 1986) and is suitable for experimentally studying the frictional properties of grain comminution in faults. Notably, large, thick experimental fault zones were observed within the granular medium. We then followed the key mechanisms of grain comminution by combining frictional measurements, post-slip structural observations, and data analyses. Finally, we propose a filling mechanism, namely the saturation and overflow of comminuted fine particles within shear zone, to interpret the transient frictional behavior.

2. Materials and Methods

Angular-shaped granular halite (NaCl) with two different initial sizes, namely coarse-grained halite (~2–5 mm) and fine-grained halite (~0.425–0.85 mm), were used as model granular materials.

The experimental setup is schematically shown in Figure 1a. The ring-shear apparatus has previously been used in the studies of landslide behavior (e.g., Sassa et al., 1996, 2004; Sassa & Lee, 1993). Detailed specifications are outlined by Sassa et al. (2004). In each test, approximately 1.5 kg of granular halite was evenly distributed in a ring-shear box (outer and inner diameters of 18 and 12 cm, respectively, with a 10.9 cm maximum sample height). The upper shear box remained stationary while the lower shear box rotated. The rubber edges were glued to the lower shear box separation to prevent grain leakage. The halite samples were sheared at a constant slip rate of

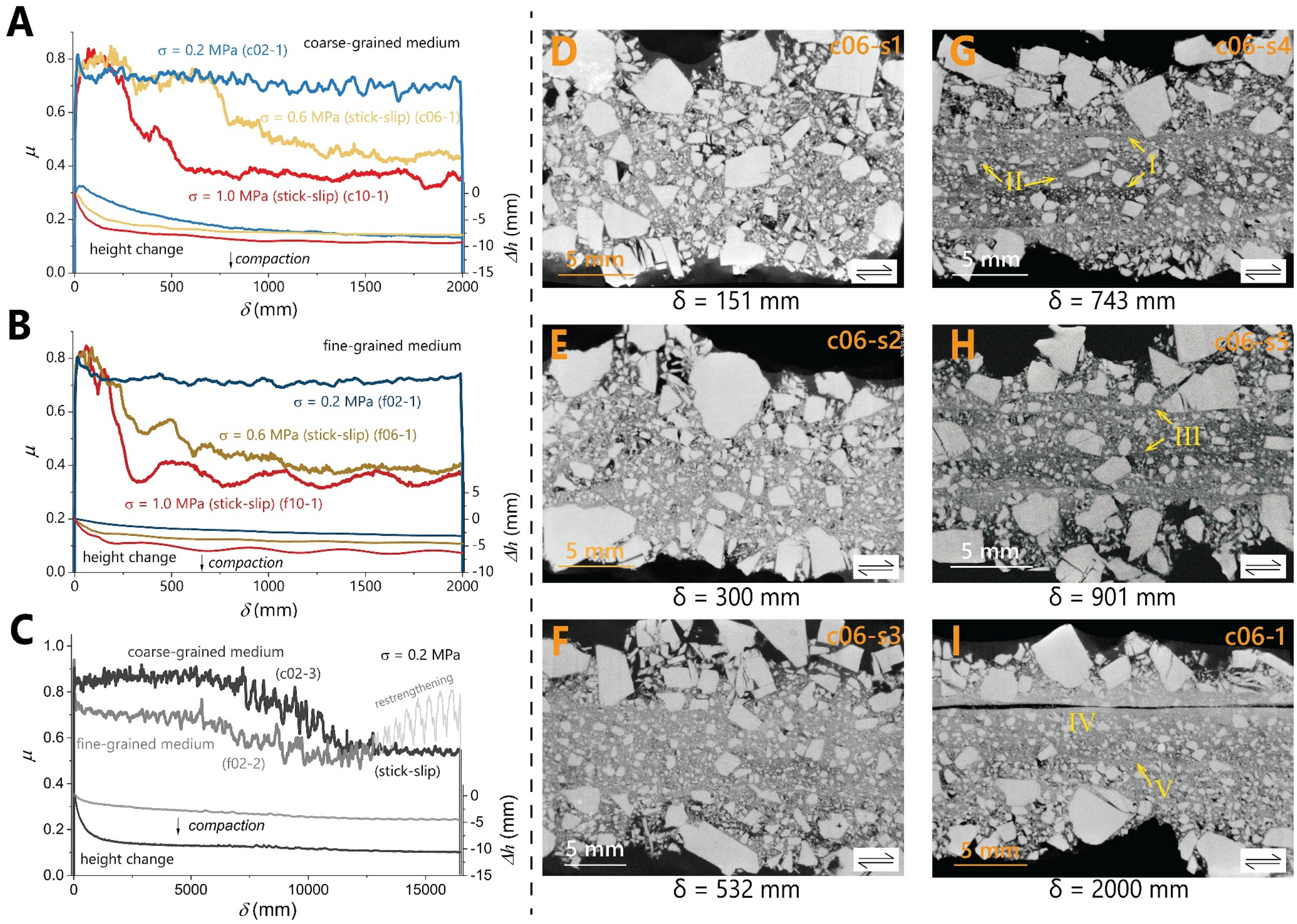

Figure 2. Representative frictional behaviors (left) and cross sections of shear zone (right). (left) Evolution of friction in runs for coarse-grained (a) and fine-grained (b) media, where the friction coefficient and height change are plotted against slip displacement under varying normal stresses. Runs for coarse and fine grains subjected to large slip displacements under 0.2 MPa (c). (right) Cross-sectional images (d)–(i) for six runs (Table S1) in which the coarse-grained samples were sheared under normal stress of 0.6 MPa to given, increasing slip displacements (δ).

0.05 cm/s under three levels of normal stress: 0.2, 0.6, and 1.0 MPa. All experimental runs were completed in room-dry conditions (humidity ~50%) at 24°C. A typical slip displacement of 2 m was applied to baseline runs (Table S1 in Supporting Information S1) unless otherwise noted. Each run resulted in a compacted ring of halite in a shear zone (box, Figure 1) within the sample column, with the center of shear zone located below the shear box separation. Six runs were performed in coarse-grained media under 0.6 MPa and stopped at different slip displacements. After each of six runs, we carefully took out blocks from the shear zone. As shown in Figures 1b and 1c, the shear-zone samples were cohesive and hardened. Post-experiment structural analyses of the halite fault zone were performed using micro-X-ray CT. More details are provided in the "Expanded Methods" section and Table S1 in Supporting Information S1.

3. Results

3.1. Frictional Behavior

Figures 2a–2c show representative frictional behavior, with the data smoothed using a moving average. Comparisons of raw and processed data are provided in the Supporting Information (Figures S1–S18 in Supporting Information S1). Here, we emphasize the evolution of the friction coefficient (μ) and sample height change (Δh) against the slip displacement (δ). In Figure 2a, all coarse-grained samples showed an increase in friction in the initial loading stage. For the run performed under the lowest normal stress ($\sigma = 0.2$ MPa), the friction coefficient reached its peak and then remained at $\mu \approx 0.7$ until the test ended. The sample exhibited dilation and switched to continuous compaction after reaching the peak friction. In contrast, under intermediate normal stress ($\sigma = 0.6$ MPa), the friction started to weaken at a slip displacement of approximately 660 mm. Finally, substantial weakening was observed at a steady-state value $\mu \approx 0.43$. In addition, the height change indicated compaction during the initial phase. Under maximum normal stress ($\sigma = 1.0$ MPa), the friction remained relatively stable for a small displacement of ~200 mm. Rapid weakening was then initiated, and friction evolved to a significantly lower value of $\mu \approx 0.36$. The results of the fine-grained media (Figure 2b) are comparable to those of the coarse-grained media. The total change in height in the fine-grained medium was smaller than that in the coarse-grained medium.

Notably, substantial weakening occurred at small displacements when the normal stress was high, indicating that the evolution of friction was dependent on the normal stress. To examine frictional weakening under the lowest normal stress (0.2 MPa), we conducted friction experiments at large slip displacements (Figure 2c). Consequently, weakening occurred after a significantly large slip displacement of ~7 m in the coarse-grained medium and ~5 m in the fine-grained medium. In some cases, re-strengthening occurred at very large slip displacements under low normal stress (e.g., run f02-2).

3.2. Microstructures

Cross-sectional images (parallel to the shear direction) of shear zones for the six runs on coarse halite under 0.6 MPa normal stress, stopped at a series of slip displacements, are shown in Figures 2d–2i. These images provide a visualization of the structural evolution over slip displacement. Note that the brightness and contrast of each image were adjusted to better visualize structural details. Brightness scales with increasing density, meaning that brighter regions are denser than darker regions. In the baseline run (c06-1) under normal stress of 0.6 MPa, frictional weakening initiated at ~660 mm and completed before 2,000 mm slip (Figure 2a). Thus, Figures 2d-2f correspond to the structures in the constant regime, while Figures 2g-2i correspond to the structures in the weakening regime. Figure 2d suggests that drastic comminution processes have commenced at small slip displacements, with voids evident between large grains, fractures appearing in larger grains, and many fine particles accumulating within a broad domain. In Figure 2e, the total volume of voids decreased, most voids were located in the upper shear zone, and discernible grain alignment occurred in the lower shear zone. The images before weakening (Figures 2d-2f) showed significant increases in the proportion of fine particles against slip. Since fine particles filled the voids, the density contrast became smaller as shearing progressed. Figure 2f shows that very few voids existed in the shear zone immediately before weakening began, and areas with oblique alignment of grains of various sizes to the horizontal can be noticed at various positions withing the cross-section, hinting at the initiation of Reidel shear. The size of fine particles was smaller than tens of microns, which is beyond the scanning resolution.

Figure 2g shows the structure immediately after the onset of weakening at 743 mm. The density of the shear zone was lower in the middle and higher near two boundaries as indicated by the relative brightness. Several discernible, localized shear planes (I) formed in locations with large density contrasts, with a more obscure, low-density shear plane in the middle. These planes are thought to be immature as they are geometrically discrete and partially throughgoing with considerable waviness. Riedel-like oblique shears (II) became more apparent. Along these immature planes, a number of large grains survived, the position of which seems to be correlated with the waviness of the shear plane. Grains away from the shear planes were significantly larger than those near shear planes.

Figure 2h shows the structure at 901 mm slip. Multiple shear planes became evident, and were relatively flat and throughgoing, dividing regions with different densities (III). In this sample, the central shear zone appeared to accommodate the most deformation because it was the most continuous and least dense of the three.

Finally (Figure 2i), one single, well-defined shear plane (IV) was observed at 2,000 mm slip by which point maximal weakening and steady-state friction had been reached. The final localized shear plane was continuous, penetrated the entire shear zone and completely separated the sample into two discrete blocks. Other immature shear planes either failed to form in this sample or vanished after the formation of the mature shear plane (V). In the region below the shear, a trace of Reidel-like structure may be preserved, while the area above is more homogeneous in structure. Additionally, the thickness of the lower region is larger than that of the top region. Density, as reflected by brightness, was very high at the boundaries of the shear plane, reflecting a structure of intensively comminuted and tightly packed particles. A small number of fine particles remained in the gap between the slip surfaces.

10.1029/2024GL109645

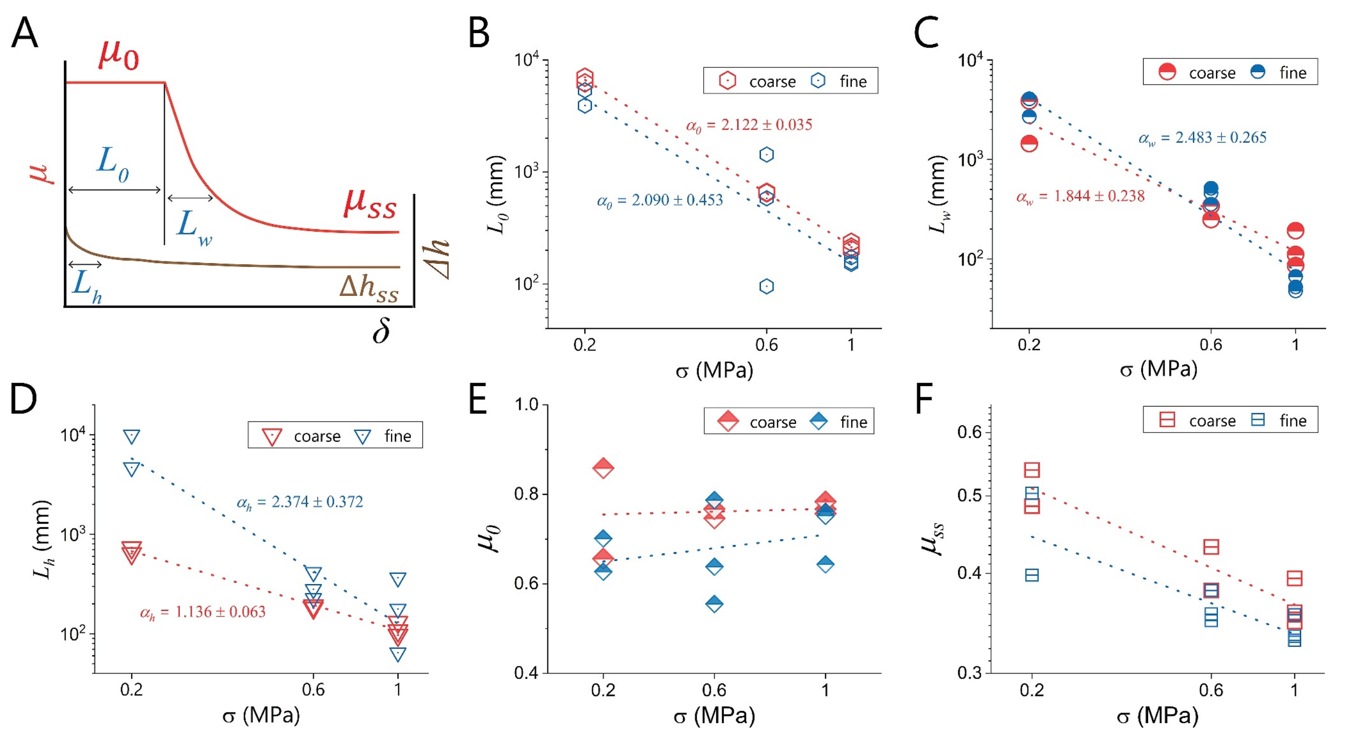

Figure 3. Effects of normal stress on frictional parameters. (a) Fitting of a frictional curve. The characteristic slip lengths for (b) the constant regime, (c) the weakening regime, and (d) compaction of the sample against normal stress. (e) Constant friction coefficient against normal stress. (f) Steady-state friction coefficient against normal stress.

4. Discussion

4.1. Data Analysis

Two distinct frictional behaviors were identified in our experimental observations, a constant friction regime followed by a regime of frictional weakening to steady state. A similar observation for crushable materials was reported by Hu et al. (2022). In Figure 3a, we illustrate the observation using a simple model of an initial constant regime followed by a weakening regime of friction with slip displacement. Frictional evolution $\mu(\delta)$ is given by the following equation:

$$\mu(\delta) = \begin{cases} \mu_0, & \delta < L_0 \\ (\mu_0 - \mu_{ss}) \exp\left(-\dfrac{\delta - L_0}{L_w}\right) + \mu_{ss}, & \delta \geq L_0 \end{cases}, \tag{1}$$

where μ_0 and μ_{ss} are the coefficients of friction in the initial and steady states, respectively, and L_0 and L_w are the characteristic slip lengths for the constant and weakening regimes, respectively.

Similarly, the equation for height change $\Delta h(\delta)$ is given by:

$$\Delta h(\delta) = \Delta h_{ss}\left[1 - \exp\left(-\frac{\delta}{L_h}\right)\right], \tag{2}$$

where Δh_{ss} refers to the steady-state value of the height change, and L_h scales the characteristic length for the height decay.

The parameters in Equations 1 and 2 were estimated using nonlinear least-squares fitting (Figures S1–S18 and Table S1 in Supporting Information S1). The characteristic lengths L_0, L_w, and L_h were plotted against normal stress σ in Figures 3b, 3c, and 3d, respectively. They are all negatively correlated to σ. We obtained $L_0 \sim \sigma^{-\alpha_0}$,

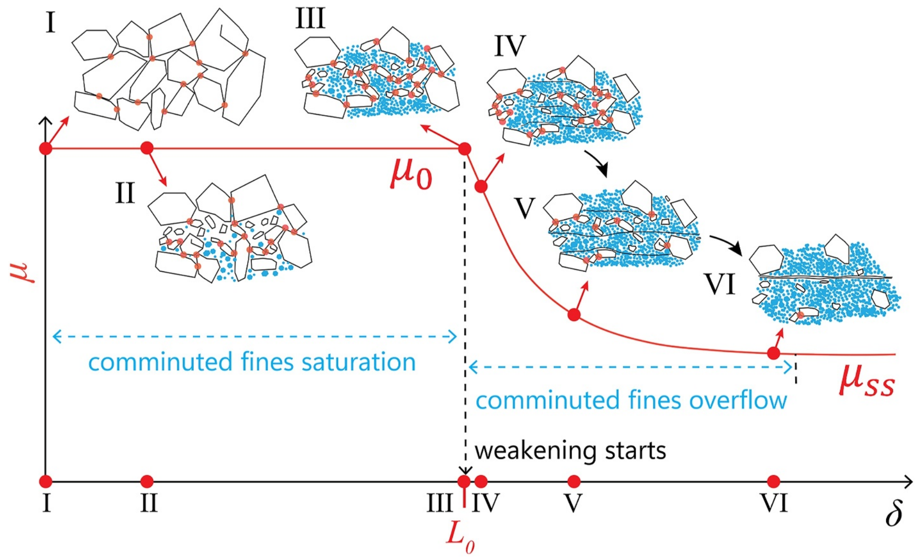

Figure 4. Depiction of transient frictional behavior and corresponding shear zone structure. Red circles denote large grain contacts and blue points represent comminuted fine particles.

$L_w = \sigma^{-\alpha_w}$ and $L_h \sim \sigma^{-\alpha_h}$, where α_0, α_w, and α_h are constants. $\alpha_0 \approx 2$ and $\alpha_w \approx 2$ were approximately obtained from the fitting, regardless of the initial grain sizes. In contrast, α_h exhibited large variability based on the grain size.

In addition, μ_0 is independent of σ (Figure 3e). This agrees with Byerlee's or Coulomb-Amonton's law of friction. In contrast, μ_{ss} decreased with increasing σ (Figure 3f), suggesting that the two regimes are governed by different physical processes. μ_{ss} was generally lower in the fine-grained medium than in the coarse-grained medium. Note that re-strengthening occurred at large slip displacements only under low-normal-stress conditions (e.g., run f02-2 in Figure S11 in Supporting Information S1). The experiments were conducted under room-dry conditions. Moisture may assist in cohesion among NaCl grains, especially when a large volume of comminuted fines is produced.

4.2. Mechanisms for Transient Frictional Behavior

Grain comminution produced numerous fine particles, filling the voids (Figures 2d-2f). Notably, friction between finely comminuted particles was markedly lower than that between larger grains (Figures 2a, 2d, and 2i). A schematic diagram in Figure 4 summarizes the evolution of frictional behavior and microstructure. We first interpret the transient frictional behaviors in the constant and weakening regimes. The next section will discuss the mechanisms for structural evolution and localization.

In the constant friction regime, large grain contacts dominate. Particularly, fine particles have the ability to migrate away from large grain contacts, as depicted in Figures 2d, 2f, and 4.

At the onset of this regime, large grains begin breaking, facilitated by their lower fracture energy consumption compared to small grains (e.g., Tavares & King, 1998; Yashima et al., 1987). Sammis et al. (1987) suggested that grains with similarly sized nearest neighbors are more prone to fracture. Thus, progressively smaller particles begin forming. As can be seen in Figures 2d–2f, the resolvable larger grains retain their angular shapes, indicating minimal shape evolution despite breaking; otherwise, spherical grains would decrease friction. The observed constant friction aligns with Mair et al. (2002), in which frictional strength remains unchanged for pervasive grain fracture of angular quartz, suggesting that friction was not strongly associated with the grain size distribution during the shear.

As grains continue breaking, smaller particles migrate into voids between larger grains, preferentially downward (Figure 4 I–III). Figure 2e shows that the voids in the lower shear zone were filled at first and rearrangement of grains occurred, suggesting the role of gravity or kinetic sieving in this process. However, the geometry of the apparatus dictates that shear concentrates near the shear box separation (Figure 1). Thus, large grain contacts remain near the separation as comminuted fine particles can migrate away from the source, maintaining constant friction μ_0. With continued shear, these voids become completely occupied by fine particles (Figure 2f). We then infer that the characteristic length L_0 is determined by the saturation of comminuted fines (Figure 4 III). When voids become unavailable for fine particle migration, the large grain contacts cease to maintain. The saturation of fine particles is accelerated under large loading, explaining decreased L_0 with normal stress (Figure 3b). Comminution and segregation processes of fine particles are likely confined within a characteristic thickness, resulting in the formation of hard shear zone blocks within the granular medium (Figures 1b and 1c). The characteristic shear-zone thickness may depend on grain size, loading condition, and geometry of the apparatus. This potentially explains the approximately 40% difference in the y-intercept of characteristic length L_0 for different initial grain sizes (Figure 3b).

We now discuss the transient frictional behavior in the weakening regime (Figure 4 III-VI). Cross-sectional images (Figures 2g–2i) reveal varying density contrasts and a reduced number of large grains. This indicates that comminution and grain rearrangement are active, though less pronounced compared to the constant regime. As voids within the characteristic thickness have been filled in the constant regime, comminuted fine particles cannot evacuate from their source, progressively reducing large grain contacts. As a result, the constant friction μ_0 decreases to the steady-state friction μ_{ss}, as fine particles contacts gradually dominate over large grain contacts. We suggest that the characteristic length L_w is determined by the overflow of fine particles (Figure 4). This overflow essentially depends on the comminution process, explaining the decreased L_w against normal stress (Figure 3c), which is characterized by a similar exponent as in the constant regime (Figure 3b).

4.3. Mechanisms for Shear Localization

Shear localization is evident in the weakening regime, where structural evolution transitions from multiple immature planes to one extremely localized plane (Figures 2g–2i). We now discuss the mechanisms responsible for this phenomenon.

In our experiments, most slips occur near the shear box separation due to the geometry of the apparatus, resulting in a shear zone where the final localized plane is positioned near this separation (Figure 1). This observation suggests the influence of geometrical constraints on the final structure. The shear zone below the localized plane appears thicker than that above it (Figure 2i), a consequence attributed to the downward migration of fine particles.

At the onset of friction weakening (Figure 4 III), voids within the shear zone become entirely filled by fine particles. However, these particles exhibit inhomogeneous distribution, a result of their migration in the constant regime, as evidenced by the density contrasts in the cross-section (Figure 2g). Slip is more likely to occur at fine particle contacts because of their lower friction compared to contacts between large grains or between large grains and fine particles. Consequently, the development of multiple discrete slip planes is initiated due to localized slips (Figure 4 IV). As fine particle contacts gradually dominate, these immature planes may coalesce or develop into flat and continuous structures (Figure 4 V). Ultimately, slips tend to concentrate on the plane closest to the shear box separation, effectively eliminating large grain contacts (Figure 4 VI). This explains the role of inhomogeneous distribution of fine particles in the formation of multiple shear planes. However, this factor alone does not fully account for preservation of only one extremely localized shear plane (Figure 2i). To further elucidate the phenomenon, mechanisms at micro-contact scale should be considered.

Bowden and Tabor (1964) suggested that the yielding of microscopic contacts is the origin of macroscopic friction during sliding. At contact points, various mechanical and chemical healing effects can increase the real contact area over time, leading to an increase in friction. These effects include creep through plastic deformation, dislocation glide, thermal activation, and pressure solution (e.g., Aharonov & Scholz, 2018; Bos & Spiers, 2002; Dieterich, 1978; Dieterich & Kilgore, 1994). Similarly, comminuted fine halite particles, when exposed to moisture, may also exhibit sensitivity to these healing effects.

During shear localization, the micro-scale contact lifetime on asperities near slip planes diminishes, hindering the potential for increased contact area by time-dependent creep. Concurrently, moisture-induced bonding effects are suppressed due to the limited time available for water diffusion at contact joints. Conversely, the healing effects become prominent in inactive regions, resulting in enhanced local strength over time.

Therefore, the uneven distribution of fine particles and healing effects trigger a feedback loop that concentrates shear strain into one final slip plane. This concentration causes multiple planes to vanish, eventually leading to the formation of one mature plane that divides the shear zone into two discrete parts. Furthermore, these healing effects can contribute to the formation of a cohesive, hardened experimental fault zone (Figures 1b and 1c). In brief, we suggest that shear localization is likely determined by geometrical constraints, particle migration, and healing effects.

4.4. Implications

The microstructures (Figures 2d–2i) resemble those observed in faults (e.g., Chambon et al., 2006; Chester & Chester, 1998; Chester & Logan, 1986; Heilbronner & Keulen, 2006; Jefferies et al., 2006) and rock avalanche deposits (e.g., Crosta et al., 2007; Davies et al., 1999; McSaveney & Davies, 2007; Perinotto et al., 2015), where layers of comminuted particles of various sizes and shapes are heterogeneously distributed in the shear zone, with indurated planes often found overlaying cohesive material (e.g., Chambon et al., 2006).

The evolution of microstructure (Figures 2d–2i) demonstrates a transition from distributed grain comminution to shear localization, accompanied by higher friction and subsequent frictional weakening, reminiscent of the similar frictional behavior observed in cataclastic flow and localized slip in triaxial halite deformation experiments (Chester, 1988; Chester & Logan, 1990). The transition of such deformation mechanisms appeared to be sensitive to normal stress and the displacement required to reach a steady state (Chester & Logan, 1990), which may be explained by the normal stress dependence on the characteristic lengths observed in our study (Figures 3b and 3c). Additionally, similar observations from different geometry and materials (e.g., Chester & Logan, 1990; Hu et al., 2022) may also be compatible with our findings.

As mentioned above, we postulated a characteristic thickness of the shear zone that accommodates both the production and filling of fine particles as well as shear localization processes. What defines this thickness? Our experiment suggests a possible answer: the shear box separation likely defined the location of the final localized shear plane, serving as the upper bound of this shear zone, while the downward particle migration defined the lower bound.

In different geological settings, the geometrical constraints can vary, and both the direction and magnitude of particle migration depend on the direction of shear and slip velocity, similar to kinetic sieving processes (e.g., Siman-Tov & Brodsky, 2018). Therefore, this thickness is strongly influenced by geometrical complexity and boundary condition in various geological contexts, further determining the characteristic length of transient frictional behavior. Additionally, the healing effects may facilitate the shear localization process by strengthening the inactive regions within the shear zone. We suggest that this characteristic thickness of the shear zone and associated characteristic length are generally applicable, given the ubiquity of grain comminution and shear localization in natural shear systems.

5. Conclusions

Friction experiments were performed on granular halite using a ring-shear configuration. We found that grain comminution is a key mechanism for determining the frictional behavior of a sheared granular system involving breakable grains. We suggest that the grain comminution generates fine particles that gradually saturate the porous shear zone in a constant friction regime, and that eventually lead to friction weakening by overflowing the shear zone and facilitating shear localization in a weakening regime. Furthermore, we observed that the intrinsic comminution and microstructure are similar to those of natural fault zones and rock avalanche deposits, indicating their relevance and significant implications for natural shear zones.

However, the underlying mechanisms remain unsolved regarding the substantially low friction between finely comminuted particles, the slope of the negative correlation between characteristic length and normal stress being equal to two, and a quantitative description of shear localization dynamics. Further studies are required to address these questions.

Acknowledgments

Important input from one anonymous reviewer, Frederick Chester, and Germán Prieto has substantially improved our work. We also thank Carlisle Landel for helpful editing, as well as Will Steinhardt, Takahiro Hatano, Heather Savage, Emily Brodsky, and Mauri McSaveney for constructive discussions, and Osamu Tadai for micro-CT measurements. We gratefully acknowledge the support from JSPS KAKENHI (JP21H05201, "Science of Slow to Fast Earthquakes").

Data Availability Statement

The complete dataset and code are available at Chang (2023).

References

Aharonov, E., & Scholz, C. H. (2018). A physics-based rock friction constitutive law: Steady state friction: A physics-based friction law. *Journal of Geophysical Research: Solid Earth*, *123*(2), 1591–1614. https://doi.org/10.1002/2016JB013829

Borg, I., Friedman, M., Handin, J., & Higgs, D. V. (1960). Chapter 6: Experimental deformation of St. Peter Sand: A study of cataclastic flow. *Geological Society of America Memoirs*, *79*, 133–192. https://doi.org/10.1130/MEM79-p133

Bos, B., & Spiers, C. J. (2002). Fluid-assisted healing processes in gouge-bearing faults: Insights from experiments on a rock analogue system. *Pure and Applied Geophysics*, *159*(11–12), 2537–2566. https://doi.org/10.1007/s00024-002-8747-2

Bowden, F. P., & Tabor, D. (1964). The friction and lubrication of solids. *Clarendon Press*, *2*(2).

Brace, W. F., & Byerlee, J. D. (1966). Stick-slip as a mechanism for earthquakes. *Science*, *153*(3739), 990–992. https://doi.org/10.1126/science.153.3739.990

Buijze, L., Niemeijer, A. R., Han, R., Shimamoto, T., & Spiers, C. J. (2017). Friction properties and deformation mechanisms of halite(-mica) gouges from low to high sliding velocities. *Earth and Planetary Science Letters*, *458*, 107–119. https://doi.org/10.1016/j.epsl.2016.09.059

Chambon, G., Schmittbuhl, J., Corfdir, A., Orellana, N., Diraison, M., & Géraud, Y. (2006). The thickness of faults: From laboratory experiments to field scale observations. *Tectonophysics*, *426*(1–2), 77–94. https://doi.org/10.1016/j.tecto.2006.02.014

Chang, C. (2023). Supplemental material for "comminution-induced transient frictional behavior in sheared granular halite" [dataset]& [Software]. *Zenodo*. https://doi.org/10.5281/zenodo.7898496

Chester, F. M. (1988). The brittle-ductile transition in a deformation-mechanism map for halite. *Tectonophysics*, *154*(1), 125–136. https://doi.org/10.1016/0040-1951(88)90230-2

Chester, F. M., & Chester, J. S. (1998). Ultracataclasite structure and friction processes of the Punchbowl fault, San Andreas system, California. *Tectonophysics*, *295*(1–2), 199–221. https://doi.org/10.1016/S0040-1951(98)00121-8

Chester, F. M., & Logan, J. M. (1986). Implications for mechanical properties of brittle faults from observations of the Punchbowl fault zone, California. *Pure and Applied Geophysics PAGEOPH*, *124*(1–2), 79–106. https://doi.org/10.1007/BF00875720

Chester, F. M., & Logan, J. M. (1990). Frictional faulting in polycrystalline halite: Correlation of microstructure, mechanisms of slip, and constitutive behavior. In *The brittle-ductile transition in rocks* (pp. 49–65). American Geophysical Union (AGU). https://doi.org/10.1029/GM056p0049

Crosta, G. B., Frattini, P., & Fusi, N. (2007). Fragmentation in the val Pola rock avalanche, Italian Alps. *Journal of Geophysical Research*, *112*(F1), F01006. https://doi.org/10.1029/2005JF000455

Davies, T. R., & McSaveney, M. J. (2002). Dynamic simulation of the motion of fragmenting rock avalanches. *Canadian Geotechnical Journal*, *39*(4), 789–798. https://doi.org/10.1139/t02-035

Davies, T. R., & McSaveney, M. J. (2009). The role of rock fragmentation in the motion of large landslides. *Engineering Geology*, *109*(1–2), 67–79. https://doi.org/10.1016/j.enggeo.2008.11.004

Davies, T. R., McSaveney, M. J., & Hodgson, K. A. (1999). A fragmentation-spreading model for long-runout rock avalanches. *Canadian Geotechnical Journal*, *36*(6), 1096–1110. https://doi.org/10.1139/t99-067

Davies, T. R. H. (1982). Spreading of rock avalanche debris by mechanical fluidization. *Rock Mechanics*, *15*(1), 9–24. https://doi.org/10.1007/BF01239474

Dieterich, J. H. (1972). Time-dependent friction in rocks. *Journal of Geophysical Research*, *77*(20), 3690–3697. https://doi.org/10.1029/JB077i020p03690

Dieterich, J. H. (1978). Time-dependent friction and the mechanics of stick-slip. In J. D. Byerlee & M. Wyss (Eds.), *Rock friction and earthquake Prediction* (pp. 790–806). Birkhäuser. https://doi.org/10.1007/978-3-0348-7182-2_15

Dieterich, J. H. (1981). Potential for geophysical experiments in large scale tests. *Geophysical Research Letters*, *8*(7), 653–656. https://doi.org/10.1029/GL008i007p00653

Dieterich, J. H., & Kilgore, B. D. (1994). Direct observation of frictional contacts: New insights for state-dependent properties. *Pure and Applied Geophysics PAGEOPH*, *143*(1–3), 283–302. https://doi.org/10.1007/BF00874332

Engelder, J. T. (1974). Cataclasis and the generation of fault gouge. *Geological Society of America Bulletin*, *85*(10), 1515. https://doi.org/10.1130/0016-7606(1974)85<1515:catgof>2.0.co;2

Faulkner, D. R., Jackson, C. A. L., Lunn, R. J., Schlische, R. W., Shipton, Z. K., Wibberley, C. A. J., & Withjack, M. O. (2010). A review of recent developments concerning the structure, mechanics and fluid flow properties of fault zones. *Journal of Structural Geology*, *32*(11), 1557–1575. https://doi.org/10.1016/j.jsg.2010.06.009

Fossen, H. (2010). *Structural geology*. Cambridge University Press. https://doi.org/10.1017/CBO9780511777806

Griggs, D., & Handin, J. (1960). Chapter 13: Observations on fracture and a Hypothesis of earthquakes. *Geological Society of America Memoirs*, *79*, 347–364. https://doi.org/10.1130/MEM79-p347

Heilbronner, R., & Keulen, N. (2006). Grain size and grain shape analysis of fault rocks. *Tectonophysics*, *427*(1–4), 199–216. https://doi.org/10.1016/j.tecto.2006.05.020

Heim, A. (1932). *Bergsturz und Menschenleben* (p. 218). Fretz und Wasmuth.

Hiraga, H., & Shimamoto, T. (1987). Textures of sheared halite and their implications for the seismogenic slip of deep faults. *Tectonophysics*, *144*(1), 69–86. https://doi.org/10.1016/0040-1951(87)90009-6

Hsü, K. J. (1975). Catastrophic debris Streams (Sturzstroms) generated by Rockfalls. *Geological Society of America Bulletin*, *86*(1), 129. https://doi.org/10.1130/0016-7606(1975)86<129:CDSSGB>2.0.CO;2

Hu, W., Xu, Q., McSaveney, M., Scaringi, G., Huang, R., Wang, G., et al. (2022). Fluid-like behavior of crushed rock flows. *Journal of Geophysical Research: Earth Surface*, *127*(10). https://doi.org/10.1029/2021JF006523

Jefferies, S. P., Holdsworth, R. E., Shimamoto, T., Takagi, H., Lloyd, G. E., & Spiers, C. J. (2006). Origin and mechanical significance of foliated cataclastic rocks in the cores of crustal-scale faults: Examples from the Median Tectonic Line, Japan. *Journal of Geophysical Research*, *111*(B12). https://doi.org/10.1029/2005JB004205

Kim, J.-W., Ree, J.-H., Han, R., & Shimamoto, T. (2010). Experimental evidence for the simultaneous formation of pseudotachylyte and mylonite in the brittle regime. *Geology*, *38*(12), 1143–1146. https://doi.org/10.1130/G31593.1

Kimura, G., Kitamura, Y., Hashimoto, Y., Yamaguchi, A., Shibata, T., Ujiie, K., & Okamoto, S. (2007). Transition of accretionary wedge structures around the up-dip limit of the seismogenic subduction zone. *Earth and Planetary Science Letters*, *255*(3–4), 471–484. https://doi.org/10.1016/j.epsl.2007.01.005

Kitajima, H., & Saffer, D. M. (2014). Consolidation state of incoming sediments to the Nankai Trough subduction zone: Implications for sediment deformation and properties. *Geochemistry, Geophysics, Geosystems*, *15*(7), 2821–2839. https://doi.org/10.1002/2014GC005360

Legros, F. (2002). The mobility of long-runout landslides. *Engineering Geology*, *63*(3–4), 301–331. https://doi.org/10.1016/S0013-7952(01)00090-4

Mair, K., Frye, K. M., & Marone, C. (2002). Influence of grain characteristics on the friction of granular shear zones. *Journal of Geophysical Research*, *107*(B10), ECV41–ECV49. https://doi.org/10.1029/2001JB000516

Mclaskey, G. C., & Yamashita, F. (2017). Slow and fast ruptures on a laboratory fault controlled by loading characteristics. *Journal of Geophysical Research: Solid Earth*, *122*(5), 3719–3738. https://doi.org/10.1002/2016JB013681

McSaveney, M., & Davies, T. (2007). Rockslides and their motion. In *Progress in landslide Science* (pp. 113–133). Springer. https://doi.org/10.1007/978-3-540-70965-7_8

Noda, H., & Shimamoto, T. (2010). A rate- and state-dependent ductile flow law of polycrystalline halite under large shear strain and implications for transition to brittle deformation. *Geophysical Research Letters*, *37*(9), L09310. https://doi.org/10.1029/2010GL042512

Noda, H., & Shimamoto, T. (2012). Transient behavior and stability analyses of halite shear zones with an empirical rate-and-state friction to flow law. *Journal of Structural Geology*, *38*, 234–242. https://doi.org/10.1016/j.jsg.2011.08.012

Perinotto, H., Schneider, J., Bachèlery, P., Le Bourdonnec, F., Famin, V., & Michon, L. (2015). The extreme mobility of debris avalanches: A new model of transport mechanism. *Journal of Geophysical Research: Solid Earth*, *120*(12), 8110–8119. https://doi.org/10.1002/2015JB011994

Polet, J., & Kanamori, H. (2000). Shallow subduction zone earthquakes and their tsunamigenic potential. *Geophysical Journal International*, *142*(3), 684–702. https://doi.org/10.1046/j.1365-246x.2000.00205.x

Robertson, E. C. (1982). Continuous formation of gouge and breccia during fault displacement. In *The 23rd U.S Symposium on rock Mechanics (USRMS)*.

Sammis, C., King, G., & Biegel, R. (1987). The kinematics of gouge deformation. *Pure and Applied Geophysics*, *125*(5), 777–812. https://doi.org/10.1007/BF00878033

Sassa, K., Fukuoka, H., Scarascia-Mugnozza, G., & Evans, S. (1996). Earthquake-Induced-Landslides: Distribution, motion and mechanisms. *Soils and Foundations*, *36*(Special), 53–64. https://doi.org/10.3208/sandf.36.Special_53

Sassa, K., Fukuoka, H., Wang, G., & Ishikawa, N. (2004). Undrained dynamic-loading ring-shear apparatus and its application to landslide dynamics. *Landslides*, *1*(1), 7–19. https://doi.org/10.1007/s10346-003-0004-y

Sassa, K., & Lee, J.-H. (1993). Measurement of the apparent friction angle during motion by the high-speed ring shear apparatus. *Landslides*, *30*(1), 1–10. https://doi.org/10.3313/jls1964.30.1

Scholz, C. H. (1987). Wear and gouge formation in brittle faulting. *Geology*, *15*(6), 493. https://doi.org/10.1130/0091-7613(1987)15<493:wagfib>2.0.co;2

Shimamoto, T. (1986). Transition between frictional slip and ductile flow for halite shear zones at room temperature. *Science*, *231*(4739), 711–714. https://doi.org/10.1126/science.231.4739.711

Shimamoto, T., Handin, J., & Logan, J. M. (1980). Specimen-apparatus interaction during stick-slip in a triaxial compression machine: A decoupled two-degree-of-freedom model. *Tectonophysics*, *67*(3–4), 175–205. https://doi.org/10.1016/0040-1951(80)90234-6

Sibson, R. H. (2003). Thickness of the Seismic slip zone. *Bulletin of the Seismological Society of America*, *93*(3), 1169–1178. https://doi.org/10.1785/0120020061

Siman-Tov, S., & Brodsky, E. E. (2018). Gravity-independent grain size segregation in experimental granular shear flows as a mechanism of layer formation. *Geophysical Research Letters*, *45*(16), 8136–8144. https://doi.org/10.1029/2018GL078486

Tavares, L. M., & King, R. P. (1998). Single-particle fracture under impact loading. *International Journal of Mineral Processing*, *54*(1), 1–28. https://doi.org/10.1016/S0301-7516(98)00005-2

Tsutsumi, A., & Shimamoto, T. (1997). High-velocity frictional properties of gabbro. *Geophysical Research Letters*, *24*(6), 699–702. https://doi.org/10.1029/97GL00503

Weeks, J. D., & Tullis, T. E. (1985). Frictional sliding of dolomite: A variation in constitutive behavior. *Journal of Geophysical Research*, *90*(B9), 7821–7826. https://doi.org/10.1029/JB090iB09p07821

Yamashita, F., Fukuyama, E., Mizoguchi, K., Takizawa, S., Xu, S., & Kawakata, H. (2015). Scale dependence of rock friction at high work rate. *Nature*, *528*(7581), 254–257. https://doi.org/10.1038/nature16138

Yashima, S., Kanda, Y., & Sano, S. (1987). Relationships between particle size and fracture energy or impact velocity required to fracture as estimated from single particle crushing. *Powder Technology*, *51*(3), 277–282. https://doi.org/10.1016/0032-5910(87)80030-X

References From the Supporting Information

Kawakata, H., Cho, A., Kiyama, T., Yanagidani, T., Kusunose, K., & Shimada, M. (1999). Three-dimensional observations of faulting process in Westerly granite under uniaxial and triaxial conditions by X-ray CT scan. *Tectonophysics*, *313*(3), 293–305. https://doi.org/10.1016/S0040-1951(99)00205-X

Raynaud, S., Fabre, D., Mazerolle, F., Geraud, Y., & Latière, H. J. (1989). Analysis of the internal structure of rocks and characterization of mechanical deformation by a non-destructive method: X-Ray tomodensitometry. *Tectonophysics*, *159*(1–2), 149–159. https://doi.org/10.1016/0040-1951(89)90176-5